Co- and postseismic deformation of the 28 March 2005 Nias M_w 8.7 earthquake from continuous GPS data

Corné Kreemer,[1] Geoffrey Blewitt,[1] and Frantz Maerten[2]

Received 21 December 2005; revised 22 February 2006; accepted 1 March 2006; published 6 April 2006.

[1] Global Positioning System (GPS) measurements registered up to >5m of coseismic displacements during the 28 March 2005 M_w = 8.7 Nias earthquake, Indonesia. The vertical offsets put tight constraints on the northern and southern limit of the rupture. The inferred coseismic slip distribution indicates high slip patches near the epicenter and near the southern extent of the 26 December 2004 Aceh-Andaman rupture, where aftershocks have been abundant. Six months of postseismic time-series are better fit with a logarithmic instead of exponential function, suggesting that the postseismic deformation is likely controlled by afterslip. Our inversion model predicts afterslip to be concentrated both up- and down-dip from patches of maximum coseismic slip where aftershocks are sparse. The shallow afterslip adds further evidence that the earthquake probably did not break the surface (with implications for tsunami generation) and instead caused aseismic deformation in shallow parts of the subduction zone after the event. **Citation:** Kreemer, C., G. Blewitt, and F. Maerten (2006), Co- and postseismic deformation of the 28 March 2005 Nias M_w 8.7 earthquake from continuous GPS data, *Geophys. Res. Lett.*, *33*, L07307, doi:10.1029/2005GL025566.

1. Introduction

[2] The M_w = 8.7 Nias earthquake of 28 March 2005 happened three months after the M_w = 9.2 December 26, 2004, Aceh-Andaman earthquake and may be the largest aftershock ever recorded. It was recorded by a network of nearby continuous Global Positioning System (GPS) stations, namely the Sumatra GPS Array (SuGAr), which did not record significant displacements related to the December event [*Subarya et al.*, 2006], but was optimally located to constrain the co- and postseismic deformation associated with the March event. Here we model the co- and postseismic slip distribution for the Nias event from the analysis of the GPS time-series (mainly) from the SuGAr array. The co- and postseismic slip models are of particular interest, because of the size of this event, its relationship to the December earthquake, and the intriguing observation that this event did not create a sizable tsunami. These models provide insight into the seismic cycle (and future hazard) along the Sumatra subduction zone in particular, and on the dynamics of large subduction-type earthquakes in general.

[3] Many studies have attributed postseismic transients in geodetic time-series to an afterslip process down-dip from the rupture [e.g., *Melbourne et al.*, 2002], but fast-decaying shallow afterslip [e.g., *Bürgmann et al.*, 2002], as well as viscous relaxation [e.g., *Pollitz et al.*, 2000] have also been invoked occasionally as plausible mechanisms, with the different processes acting over different time-scales (and probably concurrently) after an earthquake. Here we fit the postseismic time-series with simple analytical functions, which are first-order representations of afterslip and relaxation processes.

2. Co- and Postseismic Displacements

[4] Postseismic time-series for the Nias event were generated from the GPS station position estimates. These time-series were then corrected for ongoing deformation after the Aceh-Andaman event (Figure 1). (The auxiliary material[1] describes the times-series analysis in detail.)

[5] We performed a non-linear minimization scheme using the Levenburg-Marquardt method [*Press et al.*, 1992] to estimate for the December and March events the coseismic offsets and postseismic deformation parameters simultaneously. The two postseismic processes we consider independently are velocity-strengthening afterslip, which follows a logarithmic decay [*Marone et al.*, 1991],:

$$u(t) = c + a \ln\left(1 + t/\tau_{\log}\right) \tag{1}$$

and a relaxation mechanism, which in its most simplistic form (and particularly near the rupture) follows an exponential decay [*Savage and Prescott*, 1978]:

$$u(t) = c + a\left(1 - e^{-t/\tau_{\exp}}\right) \tag{2}$$

In (1) and (2) t is time since the earthquake, $u(t)$ is the position (east, north, and up), c is the coseismic offset, a is the amplitude associated with the decay, and $\tau_{\log}$ and $\tau_{\exp}$ are the logarithmic and exponential decay time, respectively, and are assumed to be similar for all time-series. We did not assume parameters a or c to be similar between (1) and (2). For stations BSIM, LEWK, LHWA, and UMLH that were installed in the few months between the Aceh-Andaman and Nias earthquakes, we solved for an additional constant velocity term in (1) and (2) and constrained τ to be that obtained from the 14 other stations. In solving for the

[1] Nevada Bureau of Mines and Geology and Seismological Laboratory, University of Nevada, Reno, Nevada, USA.
[2] IGEOSS, Montpellier, France.

0094-8276/06/2005GL025566$05.00

[1] Auxiliary material is available at ftp://ftp.agu.org/apend/gl/2005gl025566.

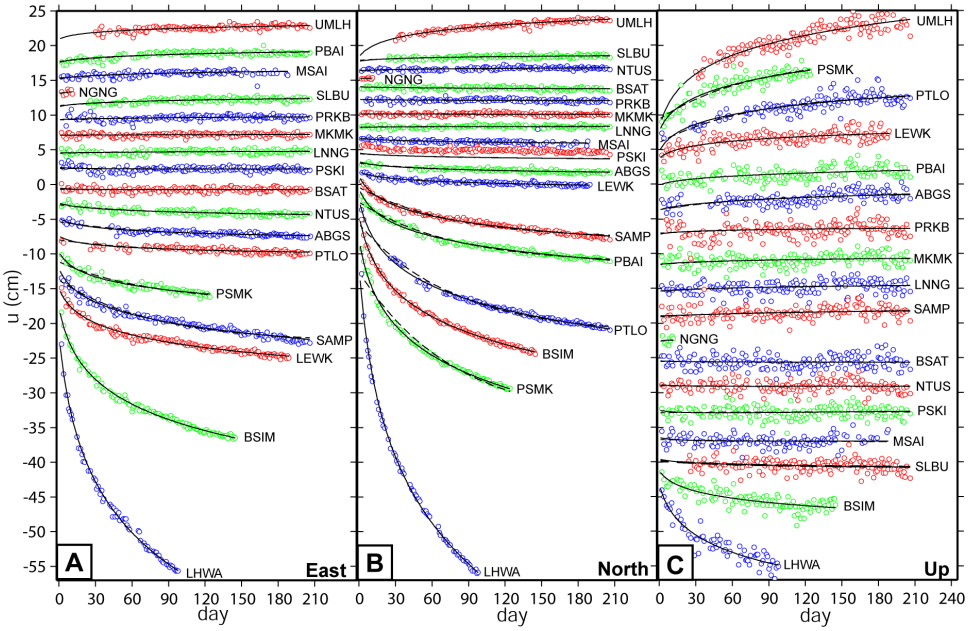

Figure 1. Postseismic time-series for the 18 analyzed stations. Note that the time-series are vertically displaced (see Table 1 for coseismic offset values). Solid and dashed lines are best-fit logarithmic and exponential functions, respectively (The relaxation predictions are not shown for newly installed stations BSIM, LEWK, LHWA, and UMLH, because the additional constant velocity that is solved for those stations differs between the two models and changes the appearance of the time-series.): (a) east direction, (b) north direction, and (c) up direction.

postseismic parameters for the March event we corrected for all stations the post 28 March 2005 times-series for the ongoing postseismic deformation related to the 26 December 2004 earthquake. For this correction we assumed that the postseismic time-series after the 2004 event is controlled by a similar (logarithmic or exponential) decay mechanism as modeled for the March event.

[6] Our estimated geodetic coseismic offsets and postseismic amplitudes for the Nias earthquake range between stations from several meters to millimeters (Figure 2 and

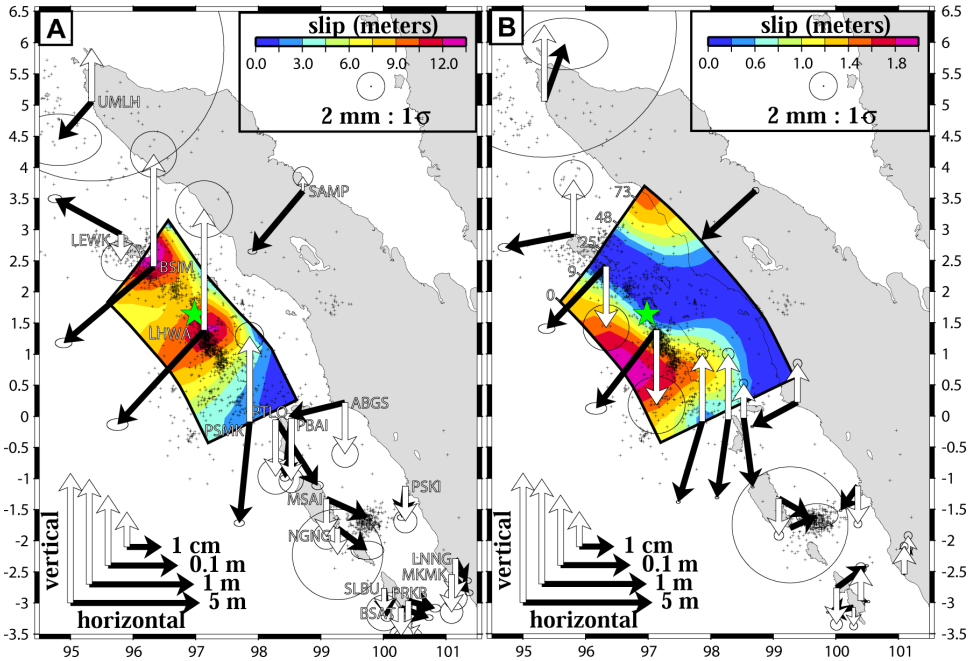

Figure 2. Horizontal (black) and vertical (white) GPS offsets, scaled with the natural log. Uncertainty ellipse is unscaled. Contours are slip magnitudes on increasingly steeper surface at depth, and crosses are aftershocks from the NEIC catalog. Green star is epicenter. (a) Coseismic, (b) postseismic from 180 days of predicted cumulative afterslip.

Table 1. Co- and Postseismic Parameters for March 28, 2005, Nias Earthquake

Site	Lon., °E	Lat., °N	c_{east},[a] mm	c_{north},[a] mm	c_{up},[a] mm	a_{east},[b] mm	a_{north},[b] mm	a_{up},[b] mm	χ_ν^{2c}	χ_ν^{2d}
abgs	99.39	0.22	−44.4 ± 0.6	−10.8 ± 0.5	−29.5 ± 0.2	−7.7 ± 0.2	−4.1 ± 0.2	3.5 ± 0.6	2.1	2.3
bsat	100.28	−3.08	6.5 ± 0.6	−2.3 ± 0.4	−6.4 ± 1.7	−1.7 ± 0.2	−0.3 ± 0.1	−1.0 ± 0.6	3.2	3.2
bsim[e]	96.32	2.41	−1809.4 ± 1.2	−1536.5 ± 0.7	1600.5 ± 3.3	−59.0 ± 0.8	−61.9 ± 0.5	−16.7 ± 2.2	3.3	10.9
lewk[e]	95.80	2.92	−121.4 ± 1.0	65.8 ± 0.6	−5.7 ± 2.8	−28.3 ± 1.0	−5.5 ± 0.6	10.4 ± 2.7	2.4	3.2
lhwa[e]	97.13	1.38	−3082.7 ± 1.5	−3356.2 ± 0.8	2870.0 ± 4.1	−121.4 ± 1.2	−157.6 ± 0.7	−41.2 ± 3.3	8.5	44.3
lnng	101.16	−2.29	2.4 ± 0.6	−4.6 ± 0.4	−13.7 ± 1.6	0.2 ± 0.2	0.5 ± 0.2	1.2 ± 0.6	2.7	2.7
mkmk	101.09	−2.54	3.7 ± 0.6	−3.8 ± 0.4	−11.8 ± 1.6	0.0 ± 0.2	0.3 ± 0.1	1.8 ± 0.6	2.4	2.4
msai	99.09	−1.33	18.1 ± 0.7	−8.1 ± 0.4	−12.0 ± 1.8	2.5 ± 0.2	−1.4 ± 0.2	−3.5 ± 0.7	2.3	2.3
ngng	99.27	−1.80	9.2 ± 2.3	−6.8 ± 1.3	−5.6 ± 6.5	1.9 ± 3.0	0.9 ± 1.7	0.4 ± 8.3	1.8	1.8
ntus	103.68	1.35	−8.9 ± 0.6	−5.6 ± 0.4	−0.1 ± 1.3	−7.7 ± 0.2	−4.1 ± 0.2	4.4 ± 0.6	4.0	4.0
pbai	98.53	−0.03	−5.4 ± 0.6	−51.6 ± 0.4	−58.9 ± 1.7	3.6 ± 0.2	−28.8 ± 0.1	4.4 ± 0.8	3.3	3.6
prkb	100.40	−2.97	6.0 ± 0.8	−1.6 ± 0.6	−15.5 ± 2.3	0.4 ± 0.3	0.0 ± 0.2	2.5 ± 0.8	3.0	3.0
pski	100.35	−1.12	−0.9 ± 0.7	−7.8 ± 0.4	−10.0 ± 1.7	−1.2 ± 0.2	−1.7 ± 0.1	−3.6 ± 0.6	2.8	2.9
psmk	97.86	−0.09	−81.3 ± 0.8	−796.3 ± 0.5	275.1 ± 2.0	−20.6 ± 0.3	−70.6 ± 0.2	26.3 ± 0.8	4.1	19.5
ptlo	98.28	−0.05	90.0 ± 0.8	−141.0 ± 0.6	−41.4 ± 2.6	−7.6 ± 0.3	−52.4 ± 0.2	21.7 ± 0.9	3.6	5.6
samp	98.71	3.62	−114.7 ± 0.7	−136.9 ± 0.4	2.6 ± 1.4	−159.6 ± 0.8	−159.6 ± 0.8	−159.6 ± 0.8	5.2	8.2
slbu	100.01	−2.77	0.7 ± 0.9	−6.5 ± 0.6	−5.0 ± 2.6	2.7 ± 0.3	2.0 ± 0.2	−3.2 ± 0.9	2.5	2.5
umlh[e]	95.34	5.05	−18.2 ± 6.2	−20.9 ± 3.7	32.4 ± 19.0	5.5 ± 7.3	15.4 ± 4.0	44.4 ± 21.	2.5	2.5

[a]Coseismic offset from (1).
[b]Decay amplitude from (1).
[c]Reduced χ^2 of fit for logarithmic decay.
[d]Reduced χ^2 of fit for exponential decay.
[e]For these sites a constant secular velocity was also included in the inversion.

Table 1). (Model parameters obtained for the December event are summarized in Table S1). With each model fitted separately, we find $\tau_{\log} = 6.2 \pm 0.1$ days and $\tau_{\exp} = 77.8 \pm 0.3$ days. The postseismic times-series are fit significantly better by (1) than (2): the data fit results in $\chi^2_\nu = 3.2$ and $\chi^2_\nu = 5.4$, respectively. The χ^2_ν for individual stations (Table 1) are for all stations better (in the near-field) or equal (in the far-field) when the logarithmic function is considered (see also Figure 1). We therefore assume for the remainder of the paper that the postseismic deformation for the 6 months since the event is dominated by afterslip, although we note that both (1) and (2) are simplifications that do not fully address the intricacies of the 3-D stress and strain fields that arise for a case with a complex slip distribution on a finite fault. The data furthermore suggest that there is no temporal variation in the spatial characteristics of the afterslip process; that is, we can assume one common decay time for all time-series combined, with single decay magnitudes for each time-series. We further note that the post 26 December 2004 time-series are fit better by (1) than (2) as well (Table S1). This result justifies our assumption to adopt a similar postseismic decay mechanism after both events when we correct the post 28 March time-series for ongoing postseismic deformation related to the December event.

3. Co- and Postseismic Slip Model

[7] The large spatial variation in coseismic offset magnitudes (Figure 2a) places strong constraints on which to build a coseismic slip model. In particular, sites that moved up during the earthquake must be situated above the rupture plane. Consequently, the northern extension of the rupture plane must lie between stations LEWK and BSIM (which is also the exact southern limit of the Aceh-Andaman rupture [*Meltzner et al.*, 2006; *Subarya et al.*, 2006]), and the southern limit must lie between PSMK and PTLO, (similar to the southern extent of the 1861 M = 8.5 rupture [*Natawidjaja et al.*, 2004]). We chose the up-dip limit of our model plane to be the trench and the down-dip width to be the 50 km slab contour [*Gudmundsson and Sambridge*, 1998]. We let the dip vary from 8° at the surface to 23° at 50 km depth.

[8] To model the coseismic slip distribution on the fault plane described above we used our coseismic offsets as data input for the Poly3Dinv code [*Maerten et al.*, 2005]. This approach is based on a solution of an angular three-dimensional dislocation in a linear, homogeneous, and isotropic elastic half-space, and during the inversion the data misfit as well as model roughness are minimized. We applied negativity constraints for left-lateral and normal slip, and set the slip to zero at the down-dip fault boundary. Our preferred coseismic slip model is shown in Figure 2a. The vertical postseismic offsets (Figure 2b) indicate that the along-trench extent of afterslip is roughly similar to that indicated by the coseismic data: the northern extent separates LEWK (which goes up) from BSIM (which goes down), and the southern extent separates LHWA (which goes down) from PSMK (which goes up). We therefore model the postseismic slip distribution on the same model surface used for the coseismic rupture, except that we extend the fault plane to larger depths to accommodate the possibility of significant deep afterslip. The decay amplitudes control the pattern of afterslip distribution and as a function of time they control the absolute magnitude of the slip distribution. We model the afterslip distribution for 180 days of accumulated postseismic deformation (Figure 2b).

4. Discussion and Conclusions

[9] The total moment from our coseismic model is M_w = 8.37 for a shear modulus (μ) of 30 GPa. This corresponds to a moment that is three times smaller than the Harvard CMT estimate. A reconciliation of these values is possible when it is assumed that μ increases rapidly with depth (e.g., μ = 100 GPa at 50 km), which is permissible [*Bilek and Lay*, 1999], and has also been argued for the 2004 Aceh-Andaman event

[*Kreemer et al.*, 2006]. In addition, if the slip were modeled using a layered Earth instead of half-space model, more slip would be predicted at greater depths, which would increase the moment estimate as well.

[10] We observe maximum coseismic slip of over 10m in two distinct regions: one near the epicenter and one near the northern extent of the rupture, abutting the southern extent of the 26 December 2004 rupture. These two maxima are located underneath stations BSIM and LHWA. The slip model is largely dominated by these two data points and so our slip model may be biased. However, our solution is similar to a recent seismic model [*Walker et al.*, 2005] in which high slip is concentrated near the same locations as in our model, adding some confidence to our result. We observe that the areas with highest slip also saw the highest aftershock activity. To test whether our chosen maximum depth of 50 km does not influence our model result, we also perform an inversion using the same fault plane as was used in the postseismic model, and the results confirm that slip below 45-50 km is negligible. The model results are however less robust as to whether and how much slip occurred near the ocean floor. We conclude that coseismic slip is constrained to the same depths that were earlier identified as being locked for the same subduction zone further to the south [*Simoes et al.*, 2004].

[11] We show that at least for over 6 months after the earthquake the postseismic times-series are very well fit by a logarithmic function. They are fit significantly worse if an exponential function is used, at least for the stations closest to the rupture. Although this statistical difference may be outweighed by our use of simple first-order representations of the various physical processes at play, we conclude that the postseismic deformation thus far has likely, but not necessarily exclusively, been dominated by afterslip. Future work will need to address the interplay of the various mechanisms [e.g., *Montési*, 2004; *Pollitz et al.*, 1998], which will lead to more sophisticated models of the earthquake process. Nevertheless, our postseismic inversion results show some characteristic patterns. Afterslip of > 1m is constrained to depths $<\sim$9 km, with an additional zone of large afterslip below the northern part of the coseismic rupture. The deep afterslip is largely controlled by BSIM. The shallow and deep regions have experienced little aftershock activity, emphasizing the aseismic nature of the afterslip process. The total slip after 180 days adds up to a seismic moment that is 50% of the main shock, equivalent to M_w = 8.17. The widespread afterslip at shallow depths is profound and either reflects creep on the actual shallow fault plane and/or relates to broad postseismic adjustment in the unconsolidated sediments. If the coseismic rupture did not reach the surface, then it is expected that stresses at shallower depths have changed in such a way that they could have driven the observed shallow postseismic deformation. If true, this scenario will contribute to understanding why the Nias earthquake did not produce a sizable tsunami.

[12] **Acknowledgments.** We thank the International GPS Service and BAKOSURTANAL for making GPS data available. We particularly wish to thank the Tectonics Observatory at Caltech and the Indonesian Institute of Sciences for establishing, maintaining and operating the SuGAr array and, with SOPAC, for archiving the data and making them available. We also thank D. Pollard for making the Poly3D programs available, and M. Chlieh and A. Meltzner for providing preprints.

References

Bilek, S. L., and T. Lay (1999), Rigidity variations with depth along interplate megathrust faults in subduction zones, *Nature*, *400*, 443–446.

Bürgmann, R., et al. (2002), Time-dependent distributed afterslip on and deep below the Izmit earthquake rupture, *Bull. Seismol. Soc. Am.*, *92*, 126–137.

Gudmundsson, O., and M. Sambridge (1998), A regionalized upper mantle (RUM) seismic model, *J. Geophys. Res.*, *103*, 7121–7136.

Kreemer, C., G. Blewitt, W. C. Hammond, and H.-P. Plag (2006), Global deformation from the Great 2004 Sumatra-Andaman earthquake observed by GPS: Implications for rupture process and global reference frame, *Earth Planets Space*, *58*, 141–148.

Maerten, F., P. Resor, D. Pollard, and L. Maerten (2005), Inverting for slip on three-dimensional dault surfaces using angular dislocations, *Bull. Seismol. Soc. Am.*, *95*, 1654–1665.

Marone, C. J., C. H. Scholz, and R. Bilham (1991), On the mechanics of earthquake afterslip, *J. Geophys. Res.*, *96*, 8441–8452.

Melbourne, T. I., F. H. Webb, J. M. Stock, and C. Reigber (2002), Rapid postseismic transients in subduction zones from continuous GPS, *J. Geophys. Res.*, *107*(B10), 2241, doi:10.1029/2001JB000555.

Meltzner, A. J., K. Sieh, M. Abrams, D. C. Agnew, K. W. Hudnut, J. Avouac, and D. H. Natawidjaja (2006), Uplift and subsidence associated with the great Aceh-Andaman earthquake of 2004, *J. Geophys. Res.*, *111*, B02407, doi:10.1029/2005JB003891.

Montési, L. G. J. (2004), Controls of shear zone rheology and tectonic loading on postseismic creep, *J. Geophys. Res.*, *109*, B10404, doi:10.1029/2003JB002925.

Natawidjaja, D. H., K. Sieh, S. N. Ward, H. Cheng, R. L. Edwards, J. Galetzka, and B. W. Suwargadi (2004), Paleogeodetic records of seismic and aseismic subduction from central Sumatran microatolls, Indonesia, *J. Geophys. Res.*, *109*, B04306, doi:10.1029/2003JB002398.

Pollitz, F. F., R. Bürgmann, and P. Segall (1998), Joint estimation of afterslip rate and postseismic relaxation following the 1989 Loma Prieta earthquake, *J. Geophys. Res.*, *103*, 26,975–26,992.

Pollitz, F. F., G. Peltzer, and R. Bürgmann (2000), Mobility of continental mantle: Evidence from postseismic geodetic observations following the 1992 Landers earthquake, *J. Geophys. Res.*, *105*, 8035–8054.

Press, W. H., S. A. Teukolsky, W. T. Vetterling, and B. P. Flannery (1992), *Numerical Recipes in FORTRAN 77: The Art of Scientific Computing*, 2nd ed., Cambridge Univ. Press, New York.

Savage, J. C., and W. H. Prescott (1978), Asthenosphere readjustment and the earthquake cycle, *J. Geophys. Res.*, *83*, 3369–3376.

Simoes, M., J.-P. Avouac, R. Cattin, and P. Henry (2004), The Sumatra subduction zone: A case for a locked fault zone, *J. Geophys. Res.*, *109*, B10402, doi:10.1029/2003JB002958.

Subarya, C., et al. (2006), Plate-boundary deformation of the great Aceh-Andaman earthquake, *Nature*, *440*, 46–51.

Walker, K. T., M. Ishii, and P. M. Shearer (2005), Rupture details of the 28 March 2005 Sumatra Mw 8.6 earthquake imaged with teleseismic *P* waves, *Geophys. Res. Lett.*, *32*, L24303, doi:10.1029/2005GL024395.

G. Blewitt and C. Kreemer, Nevada Bureau of Mines and Geology, and Seismological Laboratory, University of Nevada, Reno, MS 178, Reno, NV 89557–0088, USA. (kreemer@unr.edu)

F. Maerten, IGEOSS, Cap Omega, Rond Point Benjamin Franklin, CS3951, F-34960 Montpellier Cedex 2, France.